Proceedings of the ASME 2020 18th International Conference on Nanochannels, Microchannels and Minichannels ICNMM2020 July 12-15, 2020, Orlando, Florida, USA

ICNMM2020-13005

EFFECT OF WETTED MICROTEXTURING ON FRICTION IN MICROCHANNEL FLOW

Nastaran Rabiei¹, Carlos Hidrovo¹

¹Northeastern University, Boston, US

ABSTRACT

Microchannel flows are widely used in applications where small diffusion length scales are important. However, their inherent dimensional constrain also translates into high pumping power requirements. Inspired by nature, one possible method to reduce the large viscous pressure losses is to introduce textures in a microchannel. Depending on the interaction between the textured surface and the liquid, the microstructures can either be wetted or nonwetted. Less adhesion between solid and liquid in nonwetted state has made it popular in most of the friction reduction studies. However, in the nonwetted state, preventing liquid from penetrating into the grooves under pressurized conditions and the gas-liquid interface acting like a solid boundary open space to consider the wetted state for friction reduction as well. When dealing with the wetted state we should be aware that penetration of the flow inside the grooves can induce the pressure drag alongside the skin drag. Therefore, the wetted state will lead to a trade-off between skin and pressure drag. The aim of this work is to understand how different microtextures affect the total drag in a laminar microchannel flow. Textured microchannels with width-to-depth aspect ratios of 1, 10 and 50 and different width of the land region have been tested. In order to perform correct comparisons, the textured and baseline microchannels are designed to have the same volume. The results show that increasing the aspect ratio of the trenches introduces an extermum point in the hydraulic resistance of the microchannels. The optimum aspect ratio for the tested microchannels is 10. in which the trenches are not wide enough for streamlines to bend inside the trenches and increase the skin drag and they are not highly dense along the microchannel to reveal the negative effect of the pressure drag. On the whole, the hydraulic resistance of the textured channels is higher than the equivalent baseline for all the tested geometries.

Keywords: drag reduction, microtexturing, surface roughness, laminar boundary layer

INTRODUCTION

The behavior of flow over surfaces with either streamwise or spanwise textures has been interesting in the past few decades. The peculiarities observed in the velocity and pressure distribution can reveal the other aspects of flow over textured surfaces such as capability of drag reduction and transport augmentation [1]. In large scales, using streamwise riblets can result in about an 8% drag reduction that leads to 1.5% fuel saving in aircrafts [2]. Depending on the geometry of the textures, the behavior of the flow may change. V-shaped streamwise riblets in turbulent boundary layer showed promising results for drag reduction. Depth, spacing and curvature of the riblets were recognized as the critical parameters for drag [3]. It was shown that notched V-grooves can decrease drag when the riblets where wide and deep enough. Moreover, curvature of the riblets at the peak showed decrease in drag reduction while valley curvature increased the drag reduction.

Due to the significance of drag reduction in air and water transportations in line with fuel saving, early studies on textured surfaces were mostly done in the turbulent boundary layer. However, the large pressure drops found in micro length scales for the laminar boundary layer is also important because of the potential energy saving benefits. Nowadays, microchannels have a wide range of applications in different areas such as Lab-On-A-Chip devices, drug delivery [4] and microelectronics cooling [5]. There have also been various studies investigating both streamwise and spanwise microtextures on the surfaces as a means of drag reduction in the laminar regime. The microstructures increase the wetting surface which is expected to increase the skin drag induced by the shear forces, but the recirculation generated inside the grooves can reduce this effect. For triangular riblets the variation of the total drag is highly dependent on the sudden changes of flow velocity and pressure. Hence, the local drag coefficient will be mostly affected by these spikes at the corners [6,7]. The aspect ratio of the triangular riblets, being defined as the ratio of width to depth, has been introduced to reduce the total drag as it decreases (deeper valleys) [7]. The results of drag calculation in a channel with periodic grooves in the form of Fourier expansion on both the upper and lower walls have emphasized the inevitable role of the pressure drag as the majority contributing term in the total drag. Depending on the geometry of the grooves, contribution percentage of the pressure drag might differ and result in increase, decrease or no changes in the total drag [8].

In the case of spanwise textures, flow over periodic cavities should be considered. Solving for velocity and pressure distribution of the flow over a cavity has been considered as the basic knowledge of computational fluid dynamics (CFD) methods. The recirculation induced inside the cavity is the key factor for its drag behavior. On the one hand, the cavity helps the liquid accelerate on top of it, lowering the skin drag and compensating for the increased wetted surface area. On the other hand, the abrupt changes of the shear forces at the corners of the cavity creates pressure forces in the opposite direction of the flow [9]. Therefore, the idea of putting different cavities next to each other was suggested to alleviate the adverse effects of the sudden variations of the flow parameters in the cavity corners. Furthermore, optimization study of periodically distributed humps with the height of about the thickness of the viscous sublaver under Couette flow was done to minimize both the negative effects of increasing the wetted surface area and induced pressure gradients by recirculation, [10].

Depending on the interaction between solid and liquid, the surfaces of the textures can either be wetted or nonwetted. There should be an appropriate pressure difference sustained between the trapped air inside the textures and the liquid to maintain the nonwetted state. Considering p_{liquid} , p_{air} , γ , θ_A and w as pressure of the liquid in the channel, pressure of the air pocket inside the microtexture, surface tension, advancing contact angle and width of the trench, equation (1) can calculate the maximum static pressure that can be supported by the nonwetted state [11]. If the pressure difference goes beyond the calculated maximum value, the gas-liquid interface will start to bend inside the groove to reach the advancing contact angle. Thus the nonwetted state transitions into wetted state.

$$\Delta P_{max} = p_{liquid} - p_{air} = -\frac{\gamma \cos \theta_A}{w} \tag{1}$$

Therefore, the stability of the nonwetted state has always been an issue while trying to create hydrophobic or superhydrophobic surfaces, which makes it even more challenging under pressurized flow conditions in microchannels [12]. The wetted state is mostly well known for higher stiction between liquid and solid in which liquid impregnates the microstructures. Drag reduction in microchannels is possible in laminar regime when microstructures are built on hydrophobic surfaces. In that case, the slip velocity increases compared to when the surface is chemically hydrophobic without any structures. This is an indication of a shear-free surface that can reduce skin drag [13]. In addition to the instability, the solid

behavior of the gas-liquid interface in the nonwetted state due to contamination [14] draws the attention of the authors toward the possibility of introducing drag reduction in the wetted state.

The crucial component in the study of drag for flow inside textured channels is introducing a proper reference to compare the results. By considering the loss of flow due to drag as the average energy dissipation rate, it has been shown that the appropriate reference for each textured channel is the baseline that has the equal occupying volume [15]. On this basis, the drag reduction results in some studies may have been misinterpreted. Numerical studies on microchannels with fan-shaped ribs on side walls have shown that the textured channels have higher Poisueille number compared to the baseline [16]. Although, increasing the ratio of the ribs height to width of the parallel sides can improve the heat transfer, it will increase the Poisueille number along the microchannel [16, 17]. In addition, the offset roughness patterns can cause less pressure loss and heat transfer along the microchannel compared to the aligned pattern [Mohsen].

In this work, the effect of side trenches on pressure loss of microchannel flow have been studied in wetted state. All the experiments are performed in laminar regime and for Reynolds number between 6 to 36. Width-to-depth aspect ratio of the trenches and the width of land region have been considered as the varying geometrical parameters. Four different textured microchannels with aspect ratios of 1, 10 and 50 have been tested. The volume of all the microchannels is the same. The trenches are chosen to be perpendicular to the flow direction. The goal is to understand the physics behind what happens to pressure distribution and shear forces when there is a flow over transverse textured surfaces and how the geometry can affect the trade-off between the pressure and skin drag.

METHODS

1 Fabrication of microchannels

The replicating molds for the PDMS (polydimethylsiloxane) microchannel layouts are created through the photolithographic procedure. A silicon wafer is spin coated with SU8 2100, which is a near-UV negative photoresist. The geometry of the microchannel that needs to be transferred on the mold, has been printed as transparent parts on a photomask. The resistant is then polymerized by exposure of UV light. The unexposed parts of the resistant is removed by using developer to form microchannel layouts as protrusion on the mold. After mold hard bake, a mixture of PDMS and curing agent with the ratio of 10:1 is baked on the mold for 1 hour in 95 °C. Then the PDMS is peeled off the mold carefully. Channels are bonded to the glass using an oxygen plasma cleaner (Harrick Plasma) to make confined microchannels.

Figure 1 shows the important geometrical parameters of the textured channels including spacing between the trenches (a), width of the trench (b), depth of the trench (c), width of the land

region (w_p) and width of the equivalent baseline with the same occupying volume (W). Four different geometries for the trenches with width-to-depth aspect ratios $(AR = \frac{b}{c})$ of 1, 10 and 50 were tested for their drag behavior in laminar regime (6 < Re < 36) when the trenches are fully wetted. The depth of all microchannels are designed to be $100 \ \mu m$. As mentioned earlier, the dimensions of the trenches are calculated in a way that the textured microchannels maintain the same volume as of their equivalent baseline. The 3D model of microchannels used for experiments is depicted in Figure 2. The two pressure taps at the beginning and end of the channel are used for pressure drop measurements.

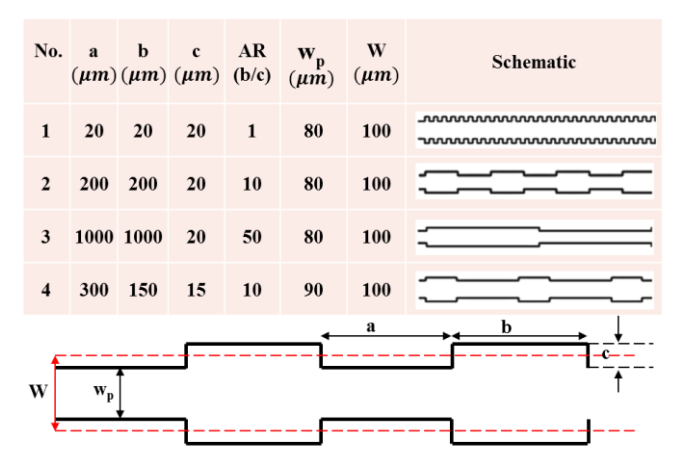


FIGURE 1: TOP VIEW OF THE TEXTURED MICROCHANNELS FABRICATED. THREE DIFFERENT ASPECT RATIOS (AR) OF 1, 10 AND 50 IS CONSIDERED. THE RED DASHED LINE REPRESENTS THE BASELINE CHANNEL THAT HAS THE SAME VOLUME AS THE TEXTURED ONE.

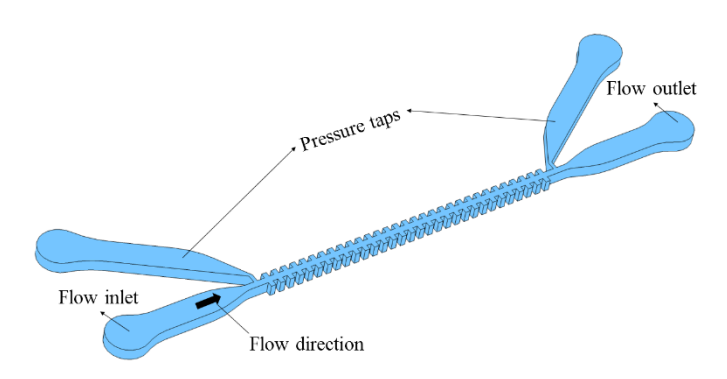


FIGURE 2: 3D MODEL OF SPANWISE TEXTURED MICROCHANNELS. THE ARROW SHOWS THE DIRECTION OF FLOW. THE PRESSURE TAPS FOR PRESSURE DROP MEASUREMENTS ARE DESIGNED AT THE BEGINNING AND END OF THE MICROCHANNEL.

2 Experimental Setup

The overall schematic of the experimental setup is shown in Figure 3. Four parameters, including liquid flow rate,

microchannel pressure drop, water temperature and channel dimensions are measured to obtain the relation between flow rate and pressure drop in microchannels. The results of each channel are then compared with the theoretical relation for the baseline. The liquid flow is supplied using a pressurized chamber. The pressure of the gas trapped inside the chamber is adjusted by a pressure regulator to control the liquid flow through the microchannel. In this study, pressure driven flow is preferred to the conventional syringe pumps to reduce the fluctuations of flow rate within time, decreasing the uncertainty of the measurements. Liquid flow rate is calculated by measuring the amount of accumulated water in the microchannel outlet over a specific time using a high precision mass scale. Two Omega differential pressure transducers with ranges of 0-1 psid and 0-5 psid and K-type thermocouple are the measurement devices used in the experimental setup. Microchannel depth and width are measured using an upright Nikon microscope with an objective of 20X and NA=0.4. A CCD camera is connected to the microscope to take images from the microchannels for record. An emphasis was made to correctly calibrate the pressure transducers to assure the accuracy of the measurements of the pressure drop along the microchannels.

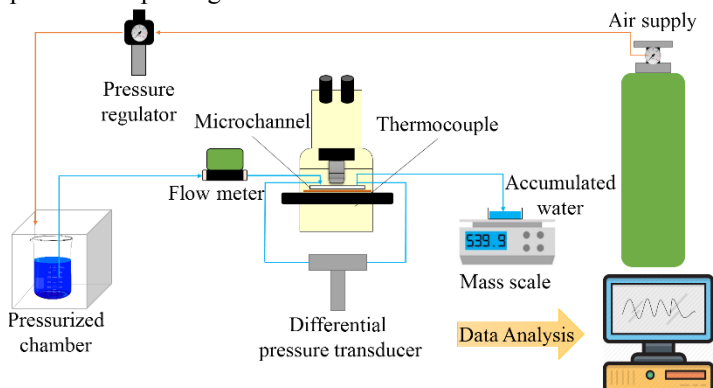


FIGURE 3: SCHEMATIC DIAGRAM OF THE EXPERIEMTNAL SETUP FOR PRESSURE-FLOW RATE MEASUREMENTS IN BASELINE AND TEXTURED MICROCHANNELS. ALTHOUGH USING MASS SCALE FOR FLOW RATE MEASUREMENTS, FLOW METER HELPS KEEPING TRACK OF FLOW RATE VARIATION OVER TIME.

3 Pressure-Flow rate characterization

The baseline microchannel is used as the benchmark to ensure the accuracy of the experimental setup and the measurements. The relation between pressure drop and flow rate for internal laminar flow is given by:

$$\Delta P = \left(\frac{Po.\mu.L}{2 A.D_h^2}\right) Q \tag{2}$$

In the equation above, ΔP is the pressure drop along the channel, A is the cross-sectional area, D_h is the hydraulic diameter, μ is the viscosity of the liquid, Q is the flow rate and L is the length of the microchannel. Friction in the microchannel is calculated using the Darcy friction factor-Reynolds number product (fRe), called the Poiseuille number (Po). The Poiseuille number is highly dependent on the channel geometry. The slope

in equation (1) can be interpreted as the hydraulic resistance (R_h) , where $R_h = \frac{\Delta P}{\rho}$. Figure 4 shows pressure drop and flow rate relation for the baseline. The measurements show a linear relation between the pressure drop and flow rate in the microchannel. The error bars include the precision errors from multiple readings and uncertainty of the measurement devices. The agreement between the experimental and theoretical results for the baseline can guarantee the accuracy of further measurements for textured channels.

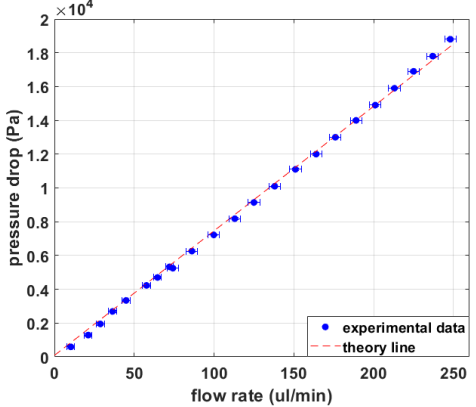


FIGURE 4: PRESSURE DROP VERSUS FLOW RATE IN A 2-CM LONG MICROCHANNEL WITH RECTANGULAR CROSS SECTION OF $100\mu m \times 100\mu m$ COMPARED WITH THE THEORY.

RESULTS

From equation (2), hydraulic resistance (R_h) can be considered as an appropriate measure of how the pressure drop varies at a specific flow rate. The larger the hydraulic resistance, the pressure drop will be large at the same flow rate indicating more pumping power requirements. In this study, some of the contributing parameters in hydraulic resistance of the tested textured microchannels remain constant. For instance, there is less than 0.1% variation in temperature that leads to less than 0.5% change in viscosity of flowing water(μ) for all experiments, which can be considered negligible. All microchannels have the same length (L). Maintaining the same volume for all microchannels, results in equal average crosssectional area(A), but not all of them will have equal hydraulic diameters (D_h) . Due to significant geometrical changes, the Poiseuille number definitely varies for each microchannel. Therefore, hydraulic resistance consists of a constant value $\left(\frac{\mu L}{2\,A}\right)$ and a variable parameter $\left(\frac{Po}{D_h^2}\right)$. In this study, the ratio of the

Poiseuille number to hydraulic diameter squared has been considered as the representative of hydraulic resistance and this variable parameter is compared for different microchannels.

The results for the four textured channels are shown in Figure 5. The error bars show how precise are the results in terms of multiple measurements that have been done during the experiments. It can be seen that for different channels the hydraulic resistance of textured channels does not change with

Reynolds number in the range that is tested (Reynolds number from 6 to 36).

In order to make sure that flow is fully developed before reaching the first trench, maximum entrance length due to maximum Reynolds number for each microchannel has been calculated in table 1. According to equation (3) the entrance length (L_e) for internal laminar flow depends on hydraulic diameter (D_h) and Reynolds number (Re_{D_h}) .

$$\frac{L_e}{D_h} \approx 0.06 Re_{D_h} \tag{3}$$

From table 1, it is implied that the design of each microchannel assures fully development of flow before the first trench. The entry region does not have any trenches and is as wide as the land region. The hydraulic diameter of each textured mirochannel is changing periodically due to the change in width of the channel in land region and textured area. Hence, the flow over trenches does not become locally fully developed. On the other hand, a repeated pattern in boundary layer growth will be formed over the land region which can indicate a state of global fully development along the microchannel. The entrance length for global fully development can be calculated using the hydraulic diameter of the equivalent baseline. The local and global fully development of the flow along the textured microchannels is not studied in detail in this work and it can be an interesting topic for future studies.

TABLE 1: MAXIMUM AND DESIGNED ENTRANCE LENGTH FOR THE MICROCHANNELS IN THE RANGE OF REYNOLDS NUMBER TESTED

Channel No.	Maximum Re	Maximum entrance length (μm)	Designed entrance length (µm)
1	30	159	305
2	23	123	432
3	18	98	1205
4	36	203	325

The results show that textured microchannels have higher hydraulic resistance compared to the baseline with the same occupying volume. This means that the pressure drop along the textured channels will be larger at a given flow rate. Despite increasing the wetted surface area, recirculation inside the trenches can increase the liquid slippage in the textured area by replacing the liquid-solid interface with liquid-liquid interface. On the other hand, the adverse pressure gradient induced by the recirculation generates pressure drag which may outweigh the skin drag in the land region. By looking at Figure 5- a, b & c one would notice that increasing the width-to-depth aspect ratio of the trenches first reduces the hydraulic resistance and then increases it. The decrease in hydraulic resistance with increasing the aspect ratio from 1 to 10 (Figure 5- a & b) happens because the number of trenches (recirculation) decreases for the same length of the channel. As the number of trenches decreases, the adverse effect of recirculation inside the trenches will gradually diminishes. The increase in hydraulic resistance with increasing the aspect ratio from 10 to 50 (Figure 5- b & c) is where the increase of wetted surface area plays a role.

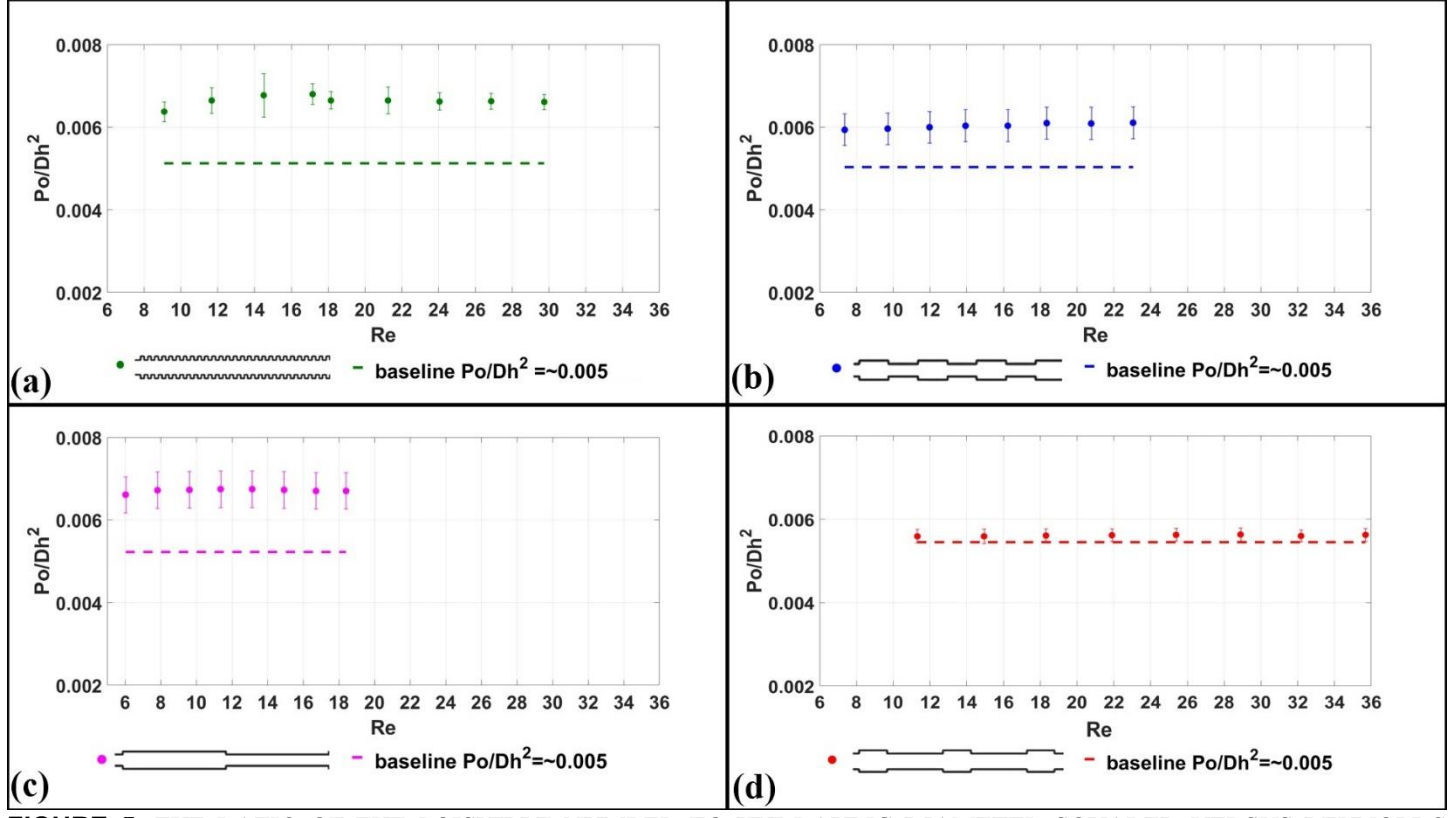


FIGURE 5: THE RATIO OF THE POISUILLE NUMBER TO HYDRAULIC DIAMETER SQUARED VERSUS REYNOLDS NUMBER FOR THE TEXTURED MICROCHANNELS (DATA POINTS) AND THEIR EQUIVALENT BASELINE (DASHED LINES) FOR HYDRAULIC RESISTANCE COMPARISON. (A) CHANNEL 1 WITH AR=1& w_p=80 μm. (B) CHANNEL 2 WITH AR=10 & w p=80 μm. (C) AR=50 & w p=80 μm. (D) AR=10 & w p=90 μm.

As the trenches become wider or shallower (high aspect ratio), the streamlines tend to bend inside the trenches and collapse the recirculation. As the result of liquid touching the bottom surface of the trenches, the skin drag increases and will turn into the main cause of overall drag increase.

Despite having the same width-to-depth aspect ratio as channel 2 (Figure 5-b), the results for channel 4 (Figure 5-d), proposes the width of the land region (w_n) as the next important geometrical parameter that should be taken into consideration for comparing the hydraulic resistance of different textured mirochannels. For the same width-to-depth aspect ratio, as the trenches become deep the width of the land region (w_n) should get smaller to maintain the same volume. Making the land region narrower leads into more hydraulic resistance which at some point will counteract the fluid slippage over the recirculation. Considering channel 4 with $w_p = 90 \,\mu m$ and channel 2 with $w_n = 80 \,\mu m$, hydraulic resistance of channel 2 is higher due to narrow land region. To sum up, the optimum aspect ratio for the tested microchannels is 10 and for this aspect ratio the closer the width of the land region to the width of the equivalent baseline, the closer the hydraulic resistance will be to that of the baseline.

CONCLUSION & FUTURE WORK

The effect of spanwise microtextures inside the microchannels on friction/drag has been investigated in wetted state. The pressure drop in this case not only stems from the shear forces, but also pressure forces appear due to the sudden changes of the flow parameters caused by the surface profile. Hence, the total drag for microchannels will be composed of two terms of skin drag (friction) and pressure drag. The recirculation induced inside the trenches can help increase the liquid slippage by changing the liquid-solid to liquid-liquid interface, which is in favor of the skin drag reduction. However, appearance of the trenches as barriers will result in unfavorable pressure drag.

The results showed that textured microchannels in wetted state in the range of Reynolds number tested (6 < Re < 36), have larger hydraulic resistance compared to the baseline that has the same occupying volume. The effect of two geometrical parameters, width-to-depth aspect ratio (AR) and width of land region (w_p) on hydraulic resistance $\left(\frac{Po}{D_h^2}\right)$ were studied. The results show that for the same w_p , as the AR increases the hydraulic resistance experiences a extermum point. It seems that decreasing the number of trenches along the microchannel by making them wider (higher aspect ratio) can help reduce the hydraulic resistance. Nevertheless, deflection of the streamlines

inside the trenches may dominate the skin drag and increase the total drag. For the textures that have the same AR, the closer the w_p to the width of the equivalent baseline, the less hydraulic resistance will be detected.

Textures with wide range of aspect ratios, including less than unity and larger than 50, can be tested for future studies to reach the optimum aspect ratio as accurate as possible. The effect of spacing between the trenches (a) can also be considered beside the other geometrical parameters. Trenches with different geometries that can mitigate the negative effects of the corners. such as curved grooves, can also be examined. Local and global fully development of the textured microchannel flow should be studied in detail. Depending on the global entrance length, multiple pressure taps can be designed in the geometry of the microchannels to examine the effect of entry length on the results. The thermal effects of the microstructures are also interesting. The advective bulk flow transport is expected to change due to the impact of microtextures on friction. Heat diffusion on the wall may be affected because of the stagnant pockets of trapped liquid. Therefore, similar to what happens between pressure and skin drag, there may be a trade-off between the advective bulk flow transport and the conduction heat transport because of the modifications that have been made on the walls of the microchannels using the trenches.

ACKNOWLEDGEMENTS

We appreciate our funding source, NSF CBET award number 1705958.

REFERENCES

- [1] Scholle, M., Rund, H., Aksel, N., 2006, "Drag reduction and improvement of material transport", Arch Appl Mech, Vol. 75, pp. 93-112.
- [2] Ball, P., 1999, "Engineering shark skin and other solutions", Nature, Vol. 400, pp. 507-509.
- [3] Walsh, M.J., 1983, "Riblets as a drag reduction technique", AIAA, Vol. 21, pp. 485-486.
- [4] Liu, D., Zhang, H., Fomtana, F., Hirvonen, J. T., Santos, H. A., 2017, "Microfluidic-assisted fabrication of carriers for controlled drug delivery", Lab on a chip, Vol. 17, pp. 1856-1883.
- [5] Hidrovo, C. H., Goodson, K. E., 2009 "Active Microfluidic Cooling of Integrated Circuits", Integrated Interconnect Technologies For 3D Nanoelectronic Systems, pp. 293-330, edited by Bakir, M. S., Meindl, J. D., Artech House.
- [6] Choi, H., Moin, P., Kim, J., 1991, "On the effect of riblets in fully developed laminar channel flow" Phys Fluids, Vol. 3, pp. 1892-1896.
- [7] Djenidi, L., Anselmet, F., Liandrat, J., Fulachier, L., 1994, "Laminar boundary layer over riblets", Phys Fluids, Vol. 6, pp. 2993–3000.
- [8] Mohammadi, A., Floryan, J.M., 2011, "Flow in grooved micro-channels" In: Proceedings of the

- seventh symposium on turbulence and shear flow phenomena (http://www.tsfp7.org), Ottawa, Canada.
- [9] Gatski, T.B., Grosch, C.E., 1985, "Embedded cavity drag in steady laminar flow", AIAA, Vol. 23, pp.1028– 1037.
- [10] Friedmann, E., 2010, "The optimal shape of riblets in the viscous sublayer", J Math Fluid Mech, Vol. 12, pp. 243–265.
- [11] Rothstein, J. P., 2010, "Slip on superhydrophobic surfaces", Annu Rev Fluid Mech, Vol. 42, pp. 89-109.
- [12] Byun, D., Kim, J., Ko, H. S., Park, H. C., 2008 "Direct measurement of slip flows in superhydrophobic microchannels with transverse grooves", Phys. Fluids, Vol. 20, 113601.
- [13] Ou, J., Rothstein, J. P., 2005, "Direct velocity measurements of the flow past drag-reducing ultrahydrophobic surfaces," Phys. Fluids, Vol.17, 103606.
- [14] Kim, T. J., Hidrovo, C., 2012, "Pressure and partial wetting effects om superhydrophobic friction reduction in microchannel flow", Phys. Fluids, Vol. 24, 112003.
- [15] Daschiel, G., Peric, M., Jovanovic, J., Delgado, A., 2013, "The holy grail of microfluidics: sub-laminar drag by layout of periodically embedded microgrooves", Microfluid Nanofluid, Vol. 15, pp. 675-687.
- [16] Chai, L., Xia, G. D., Wang, H. S., 2016, "Parametric study on thermal and hydraulic characteristics of laminar flow in microchannel heat sink with fan-shaped ribs on sidewalls Part2: Pressure drop", International Journal of Heat and Mass Transfer, Vol. 97, pp. 1081-1090.
- [17] Chai, L., Xia, G. D., Wang, H. S., 2016, "Parametric study on thermal and hydraulic characteristics of laminar flow in microchannel heat sink with fan-shaped ribs on sidewalls Part1: Heat transfer", International Journal of Heat and Mass Transfer, Vol. 97, pp. 1069-1080.